High-resolution, unstructured meshes for hydrodynamic models of the Great Barrier Reef, Australia

Sébastien Legrand [a,b,1], Eric Deleersnijder [a,b], Emmanuel Hanert [a,b], Vincent Legat [b] and Eric Wolanski [c]

[a] *G. Lemaître Institute of Astronomy and Geophysics (ASTR), Université catholique de Louvain. 2, Chemin du Cyclotron. B-1348 Louvain-la-Neuve, Belgium.*

[b] *Centre for Systems Engineering and Applied Mechanics (CESAME), Université catholique de Louvain. 4, Avenue Georges Lemaître. B-1348 Louvain-la-Neuve, Belgium.*

[c] *Australian Institute of Marine Science (AIMS), PMB No. 3, Townsville MC, Queensland 4810 Australia*

Abstract

Accuracy and mesh generation are key issues for the high-resolution hydrodynamic modelling of the whole Great Barrier Reef. Our objective is to generate suitable unstructured grids that can resolve topological and dynamical features like tidal jets and recirculation eddies in the wake of islands. A new strategy is suggested to refine the mesh in areas of interest taking into account the bathymetric field and an approximated distance to islands and reefs. Such a distance is obtained by solving an elliptic differential operator, with specific boundary conditions. Meshes produced illustrate both the validity and the efficiency of the adaptive strategy. Selection of refinement and geometrical parameters is discussed.

Key words: Unstructured grids, Great Barrier Reef, Delaunay triangulation, Finite elements methods, Finite volumes methods

[1] Corresponding author — *Email address:* legrand@astr.ucl.ac.be

1 Introduction

The Great Barrier Reef comprises over 2800 individual reefs spread over 2600 km length of the Australia's north-eastern continental shelf, at the western margin of the Coral Sea. The topography is highly complex, with individual reefs ranging in area from 0.01 to 100 km^2. In some regions, the reefs form a ribbon separated by narrow passages, and occupy approximately 90% of the along-shelf length, thus providing a significant barrier to the water flow. In other regions, the reefs are widely scattered, separated by wide passages and occupy only about 10% of the along shelf length.

The complex topography, the wind, the tides, and the circulation in the adjoining Coral Sea strongly influence the circulation on the Great Barrier Reef shelf. The latter plays a crucial role in a number of important biological processes, including the flushing of Great Barrier Reef waters by Coral Sea waters (Wolanski and Spagnol, 2000; Brinkman et al., 2002; Wolanski et al., 2003b), the connectivity of reef populations as a result of the transport of waterborne larvae between reefs (Wolanski et al., 1997; Armsworth and Bode, 1999; Wolanski et al., 2004) or the transport of nutrients and pollutants by water currents (Done, 1988; Bell and Elmetri, 1995; Wolanski et al., 1999). These processes occur over a wide range of scales in both space and time, ranging from meters to hundreds of kilometers, and from minutes to years (Wolanski et al., 2003a).

Among the small scale processes that should be simulated by an eco-hydrodynamic model of the Great Barrier Reef, there are tidal jets and eddies that occur in the wake of islands. Their length scales range from about hundred meters to a few kilometers. However, in situ measurements, satellite imagery and small-scale numerical simulations show that those phenomena are mainly confined to the neighbourhood of small reefs, islands and passages (Hamner and Hauri, 1981; Wolanski et al., 1988; Wolanski and Hamner, 1988; Deleersnijder et al., 1992; Wolanski et al., 1996). The mesh resolution should therefore be increased up to 10 or 100 m only in those regions while it can be much coarser (up to a few kilometers) in a large fraction of the Great Barrier Reef.

Nowadays, the computational power required to model the whole Great Barrier Reef with a 100 m uniform mesh is hardly affordable. For instance, the state-of-the-art numerical model of the whole Great Barrier Reef has a 2 $km \times 2$ km uniform grid (Brinkman et al., 2002). Therefore, the use of a variable-resolution mesh seems to be a better strategy. This may be achieved either with nested structured grids or with unstructured variable-resolution meshes. The former have the advantage of retaining the inherent simplicity of structured meshes while allowing variable resolution. However, the topography of the Great Barrier Reef is so complex that the implementation of an

efficient nested-grid model is likely to be extremely difficult.

On the other hand, the flexibility of unstructured meshes is such that they are able to represent complex coastlines to a high degree of accuracy. In addition, it is possible to build an unstructured mesh in which the ratio of the length of largest elements to that of the smallest is of the order of 100. Therefore, as unstructured mesh marine modelling now is a rapidly growing field of research (Hanert et al., 2005; Walters, 2005; Pietrzak et al., 2005), it is conceivable to develop an unstructured mesh numerical simulation tool of the whole Great Barrier Reef allowing for high space resolution only in regions where this is needed. The first step towards such a model is the construction of appropriate unstructured meshes of the Great Barrier Reef. The original contribution of this paper lies less in the development of an unstructured mesh generator (see Appendix A) than in the design of high-resolution, graded unstructured meshes suitable for the eco-hydrodynamic numerical simulation of the whole Great Barrier Reef. Indeed, although most refinement strategies used in marine numerical modelling are based on the bathymetry (Henry and Walters, 1993; Foreman et al., 1995; Jarosz et al., 2005; Walters, 2005), none of them are able to produce meshes suitable to accurately simulate the eddies and the jets in the neighbourhood of the islands and reefs. Therefore, the guiding principle of the refinement strategy presented in Section 2 consists in blending both a requirement related to the depth of the water column and a requirement related to the distance to the coast and reefs. As explained in Section 3, due to the complexity of the geometry of the Great Barrier Reef, this distance is estimated by solving an elliptic differential operator with specific boundary condition. Then, three gauges of mesh quality are introduced in Section 4. Finally, high-resolution unstructured meshes covering the $2.11 \times 10^5\ km^2$ of the domain of interest are discussed in Section 5.

2 A refinement strategy for the Great Barrier Reef

When designing a mesh for numerical simulations within a particular domain, a refinement strategy has to be defined to what the accuracy of the discrete representation of the unknown fields is prescribed. For the Great Barrier Reef, this target accuracy mainly depends on two major physical features: the small recirculation eddies occurring in the wake of islands and reefs, and the tidal waves propagating throughout the whole Great Barrier Reef.

Fundamental to the method of mesh adaptivity is the definition of a metric which describes the relevant requirements for the size and the shape of the elements of the mesh. The metric contains the full description of the mathematical isomorphism linking the reference equilateral element and each physical element of the mesh. Since no relevant information to design anisotropic

meshes can be easily obtained from the bathymetric field, we only focus on isotropic elements. For those meshes, the metric is fully defined by a simple scalar characteristic length: the *target element size* $h(\mathbf{x})$. This function of the position $\mathbf{x}$ provides the characteristic length of the element where $\mathbf{x}$ is located. Obviously, it is an ideal goal that cannot be perfectly satisfied as other constraints on the mesh generation procedure also apply.

In practice, this target size can be defined either a priori from the knowledge of the physics of the problem or a posteriori with an error estimator from a discrete solution computed on a given mesh. However, we do not intend to present dynamically adjusted meshes throughout the course of the integration in response to the solution of a given problem. Even if such an adaptive scheme could appear very attractive, the global handling of a dynamically adaptive calculation requires major modifications of the flow solver. Therefore, the realistic challenge consists in the design of a graded unstructured mesh from the eco-hydrodynamic physics of the Great Barrier Reef.

On the one hand, it is well known that the external inertia-gravity wave celerity is approximatively given by $\sqrt{g\,D(\mathbf{x})}$ where g and $D(\mathbf{x})$ are the gravitational acceleration and the water column depth, respectively. Our design strategy is based on the assumption that an efficient mesh would exhibit a local element size proportional to this tidal wave velocity (Henry and Walters, 1993). It consists in adjusting the resolution in such a way that, over a given time interval, external inertia gravity waves travel over a distance representing roughly the same fraction of the mesh size. As a result, a coarse mesh can be used to simulate the tide propagation in very deep areas and a finer discretisation is required in shallower regions. Such a requirement can be expressed as follows:

$$\frac{h(\mathbf{x})}{h_{max}} = \sqrt{\frac{D(\mathbf{x})}{D_{max}}},$$

where h_{max} denotes the maximal prescribed element size and D_{max} denotes the maximal value of the depth field.

On the other hand, the size of recirculation eddies that develop downstream of headlands or narrow passages is of the order of hundreds to thousands of meters. Therefore, in the regions where those eddies are likely to occur, the element size must be sufficiently small: h_{min} should range from 50 m to 100 m.

In order to take into account both requirements, we define a *blending function* $\phi(d)$ based on the distance $d(\mathbf{x})$ to the islands and reefs. This blending function vanishes in the vicinity of the islands and reefs, is equal to one in remote areas and connects both parts in a continuous and smooth way. With the help of

such a blending function, the target element size is then defined as:

$$h(\mathbf{x}) = h_{min} + \phi\Big(d(\mathbf{x})\Big)\,\sqrt{\frac{D(\mathbf{x})}{D_{max}}}\,(h_{max} - h_{min}). \tag{1}$$

A major ingredient of the mesh design is the purely heuristic definition of the blending function and the computation of the distance of each location to the closest island or reef. As a typical blending function, we use a piecewise cubic polynomial:

$$\phi(d) = \begin{cases} 0 & 0 \;\leq\; d \;\leq d_0, \\ 3\left(\frac{d-d_0}{d_1-d_0}\right)^2 - 2\left(\frac{d-d_0}{d_1-d_0}\right)^3 & d_0 \leq\; d \;\leq d_1, \\ 1 & d_1 \leq d, \end{cases} \tag{2}$$

where d_0 defines the length of a plateau along the islands in which the element size is precribed to h_{min}. Similarly, the discretisation is fully prescribed by the tidal wave velocity at a distance from the islands larger than d_1. In the transition area of width $d_t = d_1 - d_0$, the refinement is obtained as a compromise characterized by the blending function between the tidal wave velocity requirement and the necessity to ensure a smooth transition between both previous regions. The blending function and its geometrical parameters are illustrated in Figure 1.

In order to illustrate this refinement strategy, let us restrict ourselves to the simple example shown in Figure 2. A typical bathymetry profile has been extracted from the data of the Great Barrier Reef. In one dimension, it is easy to compute the distance to the coastline at the left-hand side and to the two reefs that are located next to the other side. As can be seen in Figure 2, it is then possible to define the element target size and to generate a Delaunay-like triangulation along a strip domain. However, estimating the *island distance* $d(\mathbf{x})$ for a two-dimensional problem can be very expensive and difficult.

3 A boundary value problem for the island distance

In view of the complexity of the geometry of the Great Barrier Reef, we reject the naive approach that consists in calculating Euclidian distances to every island. Inspiration has been sought in the methods other Authors have developed to tackle similar problems. Some of them had recourse to a phenomenological boundary value problem to obtain an estimated distance to a given boundary in a two-dimensional or three-dimensional domain (Assaker,

1998; Assaker et al., 1997; Brasseur et al., 1996). Typically, such an issue occurs in turbulent flow calculations involving a mixing length. According to those models, the size of large turbulent eddies at a given location is directly proportional to the distance to the wall. It is not surprising that the most efficient techniques are based on elliptic partial differential equations. Unfortunately, the most efficient partial differential equations which produce the best approximation are often highly non-linear and their resolution would be prohibitive such that we have developed our own two-step approach to obtain an approximated island distance.

Firstly, we define an island and reef proximity indicator that we call the *shore proximity function* $\sigma(\mathbf{x})$ as the solution of the following linear boundary problem:

$$\begin{cases} \mu^2 \ \boldsymbol{\nabla}^2\sigma - \sigma + 1 = 0 & \\ \sigma = 0 & \text{on islands and reefs} \\ \mathbf{n} \cdot \boldsymbol{\nabla}\sigma = 0 & \text{on other boundaries} \end{cases} \tag{3}$$

where $\mathbf{n}$ is the outward unit normal to the boundary. The stiffness length μ in front of the elliptic operator sets the length of the smooth transition from $\sigma = 0$ along the islands and reefs to $\sigma = 1$ in remote areas. In addition, the shore proximity function lies in the interval $[0, 1]$ as is demonstrated in Appendix B.

In a second step, we correlate the estimated island distance and this shore proximity function. To motivate this, let us consider the shore proximity function and the island distance in an one-dimensional semi-infinite domain with an island at the location $x = 0$. The distance coincide with the space coordinate x and the analytical solution for the shore proximity problem can be easily derived:

$$\begin{aligned} d(x) &= x, \\ \sigma(x) &= 1 - e^{-x/\mu}. \end{aligned}$$

By directly extrapolating the correlation existing for this simplified geometry, we may express the island distance in terms of the shore proximity function:

$$d(\mathbf{x}) = -\mu \ \ln\Big(1 - \sigma(\mathbf{x})\Big). \tag{4}$$

Let us here mention that such an equation is an approximation of the true connection between the shore proximity function and the island distance. The latter can be easily evaluated.

In order to better grasp the meaning of the estimated island distance, it is possible to combine both Equations (3) and (4) to show that d is in fact the solution of the following non-linear elliptic problem:

$$\begin{cases} \mu\ \boldsymbol{\nabla}^2 d - \boldsymbol{\nabla} d \cdot \boldsymbol{\nabla} d - 1 = 0 & \\ d = 0 & \text{on islands and reefs} \\ \mathbf{n} \cdot \boldsymbol{\nabla} d = 0 & \text{on other boundaries} \end{cases} \tag{5}$$

The above problem again exhibits a second-order elliptic operator and a non-linear dissipative term with the suitable boundary conditions. It is important to note that the stiffness length allows us to monitor the impact of the smoothing effect of the Laplacian term. In a simple intuitive statement, it can be stated that such a parameter can be viewed as the result of how the requirement of smoothness and the requirement of accuracy is balanced in the estimated island distance. Finally, our two steps approach allows to substitute the resolution of the non-linear boundary value problem (5) by the linear one (3).

The stiffness length μ influences the estimated island distance. On the one hand, a small stiffness length better incorporates small-scale geometrical features in the neighbourhood of the islands and reefs, but the accuracy of the distance everywhere else is quite poor. In other words, the estimated distance tends very quickly to a constant limit value. On the other hand, a large stiffness length prevents this but smooths all small geometrical features along the islands and reefs. All the tests we conducted suggest that selecting 4 km as the value of the stiffness length offers a satisfactory compromise for most applications. Therefore, the estimated island distance is calculated with this value.

In Figure 3, the Great Barrier Reef domain is divided into three regions as a function of the calculated island distance d in kilometers: $[0, 3], [3, 30], [30, \infty]$. Typically, we identify the islands and the reefs neighbourhood, the transition part and the remote region as the three parts of the support of the blending function defined in Equation (2). As a result, the geometrical parameters for the blending function are defined as follows: $d_0 = 3\ km$ and $d_1 = 30\ km$. Finally, note that we decide not to refine along the Australian coastline and the shelfbreak, in this calculation.

4 Gauges to evaluate the mesh quality for the Great Barrier Reef

The role of the mesh generator is to create the grid that provides the best numerical accuracy for a given number of degrees of freedoms. Basically, the target element size requirement has to be satisfied along with two other important constraints. For most discretisation techniques like finite volumes or finite elements, it is necessary to avoid large local discrepancies in element sizes. The second key-point is to estimate element equilaterality in the suitable metric. In this section, we define three quality gauges to analyze the geometrical quality of our generated meshes for the Great Barrier Reef.

4.1 The grading gauge

Local element size discrepancies will mainly appear in the transition area of the blending function. Therefore, it can be expected that the grading gauge measuring such local discrepancies could be directly estimated from the design parameters h_{min}, h_{max} and $d_t = d_1 - d_0$. Those three constants characterize the sharpness of the target element size function $h(\mathbf{x})$.

The *grading gauge* α is defined as a characteristic size ratio between adjacent elements in the most graded transition areas. In a one-dimensional geometrical distribution of element sizes h_i ranging from h_{min} to h_{max} in an interval of length d_t, the following relations hold :

$$\begin{aligned} h_{i+1} &= \alpha\ h_i, & i = 0, 1, ..., n \\ h_0 &= h_{min}, \\ h_n &= h_{max}\ = \alpha^n h_{min}. \end{aligned}$$

Hence, the geometrical distribution requires:

$$d_t = h_{min}\ \sum_{i=1}^{n-1} \alpha^i,$$

$$d_t = h_{min}\ \frac{\alpha - \alpha^n}{1 - \alpha},$$

$$d_t = h_{min}\ \frac{\alpha}{1 - \alpha} - h_{max}\ \frac{1}{1 - \alpha} \simeq h_{max}\ \frac{1}{\alpha - 1},$$

where n, the number of elements in the interval, is assumed to be relatively large for the last approximation.

In terms of the design parameters, we can then write the grading gauge in the closed form:

$$\alpha = \frac{d_t + h_{max}}{d_t + h_{min}}. \tag{6}$$

Limiting the grading gauge is required to avoid large local element size discrepancies, but inhibits the advantages of a non-uniform mesh only refined in areas of interest.

4.2 The shape gauge

The Delaunay-like triangulation algorithm is based on the idea that a good computational mesh is made of unitary equilateral triangles in a suitable metric. However, in the physical domain, the corresponding mesh may be highly anisotropic, even if it is not considered in this paper. Following Dompierre et al. (2003), the local shape measure of an element Ω^e is given by a normalized dimensionless *shape gauge* β_e:

$$\beta_e = \frac{\sqrt{3\ b^e \prod_{i=1}^{3} (b^e - 2\ b_i^e)}}{\left(b^e \ \max_i \ b_i^e \right)} \ , \tag{7}$$

where b_i^e and $b^e = b_1^e + b_2^e + b_3^e$ are the lengths of the edges Γ_i^e of the element Ω^e and its perimeter in the metric space defined by the target element size:

$$(b_i^e)^2 = \int_{\Gamma_i^e} \frac{1}{h^2(\mathbf{x})}\ d\Gamma \ \ . \tag{8}$$

From a geometrical point of view, the shape gauge can be viewed as a normalized ratio of the radius of the inscribed circle of the triangular element Ω^e with respect to its perimeter. The normalization ensures that the shape gauge lies in the interval $[0, 1]$ and is maximal for the ideal case: an equilateral triangle in the metric space.

Finally, we define a global shape index β as the mean value of the local shape indexes of all elements of the mesh. The mesh is usually built in such a way that the value of b_i^e is close to unity at the end of the site insertion procedure

(Frey and George, 2000). All the characteristics of the final mesh are therefore contained in the target element size field $h(\mathbf{x})$.

4.3 The edge gauge

The Watson-Bowyer algorithm does not ensure the strict respect of the target element size prescribed. In fact, it only tends to produce the mesh such that all lengths of the edge are close to unity in the metric defined by $h(\mathbf{x})$.

The discrepancy between the prescribed length and the final length of the edge Γ_f obtained by the generator is measured by a normalized dimensionless *edge gauge* γ_f:

$$\gamma_f = 1 - |b_f - 1| \quad , \tag{9}$$

The normalization ensures that the edge gauge lies in the interval $[0, 1]$ and is maximal for the ideal case: $b_f = 1$, i.e. when the obtained length is in perfect agreement with the target element size field. Finally, we define a global edge index γ as the mean value of the local indexes of all edges of the mesh.

Figure 4 shows that the selection of the transition distance d_t strongly influences the distributions of both shape and edge gauges. In particular, the selection of the mesh design parameters to reach a grading gauge $\alpha = 1.3$ is a good compromise between the number of elements and the geometrical quality of mesh estimated by those three gauges.

5 Results

The methodology and the gauges introduced above have been used for generating high resolution unstructured meshes for the Great Barrier Reef in an automatic way using our own implementation of the Watson-Bowyer algorithm.

In Figure 5, two recursive close-up views on Whitsunday islands illustrate the performance of our technique. The design parameters of this first example are $h_{min} = 1\ km$, $h_{max} = 20\ km$, $d_0 = 3\ km$ and $d_t = 62\ km$ selected in such a way that the grading gauge α is 1.3. This example illustrates the ability of generating high quality graded unstructured meshes for the Great Barrier Reef. It also illustrates the graded mesh usefulness. Indeed, the gradual mesh refinement in the neighbourhood of islands and reefs concentrates most degrees of freedom on those area during a simulation. It must be noted that 82% of

the degrees of freedom is concentrated in the area close to islands and reefs. By contrast, less than 1% of the degrees of freedom covers more 25% of the whole domain in remote regions. Here, we have assumed that the number of variables of an eco-hydrodynamical model defined on a given mesh is directly related to the number of nodes, edges and elements of the mesh. Therefore, the density of the mesh can be correlated with the number of degrees of freedom of the upcoming models. Typically, a uniform mesh would require four times more elements to cover the whole domain with a characteristic size $h = h_{min}$.

The total amount of elements and their repartition into the three regions defined by the blending function depend on the mesh design parameters. As shown in Figure 6, the relative importance of the three regions is directly linked to the selection of d_0 and d_t. Typically, the merging of adjacent islands and reefs neighbourhoods explains the appearance of a plateau in the surface occupied by the region close to islands, for an increasing value of d_0. On the other hand, the relative importance of the transition area is directly related to the value of d_t and becomes largely predominant for a large transition distance. In order to maintain the computational advantage of a graded mesh, it is therefore mandatory to limit d_t to about 30 km. Logically, the relative importance of the remote regions behaves in an opposite way.

h_{min}	h_{max}	d_0	d_t	α	β	γ	number of elements	number of edges	number of nodes
0.4 km	20.0 km	3.0 km	64.9 km	1.3	0.88	0.87	864 670	1 304 356	438 746
0.2 km	10.0 km	3.0 km	32.5 km	1.3	0.86	0.87	2 873 444	4 323 308	1 448 837
0.1 km	5.0 km	3.0 km	16.2 km	1.3	0.87	0.87	10 196 233	15 319 277	5 141 817

Table 1 : Characteristic dimensions of the meshes of Figure 6.

Table 1 gives the characteristic dimensions of some meshes with the corresponding global gauges. In particular, we emphasize that is possible to build a whole family of meshes for the Great Barrier Reef with a same grading gauge $\alpha = 1.3$. Those meshes have been obtained with several minimal and maximal element sizes in kilometers $(h_{min}, h_{max}) = (0.4, 20.0),\ (0.2, 10.0)$ and $(0.1, 5.0)$. It allows mesh refinement analysis and hierarchical eco-hydrodynamical modelling of the domain. Figure 6 shows two recursive close-up views for this family of meshes.

At this stage, it is important to discuss the data used for generating our meshes: the bathymetric field. The domain covers $2.11 \times 10^5\ km^2$ from the Australian coastline to the shelfbreak and from Rockhampton to Cape Direction. Fortunately, high-resolution ($500\ m \times 500\ m$) bathymetry data from Lewis (2001) are available. The bathymetry field exhibits sharp gradients from the occurence of islands and reefs with a relatively smooth slope from the continental shelf. First of all, the position of the Australian coastline and islands is deduced by drawing the isobath corresponding to $0\ m$. The position of the reefs and the shelfbreak is deduced from the 10-meters and the 200-meters isobaths respectively. Finally, the bathymetry has also been used to estimate the tidal wave celerity used for the target element size. In view of the high gradients, it appears useful to use a smoothed bathymetry field $\widetilde{D}(\mathbf{x})$ for our refinement strategy. In fact, this modified bathymetry is obtained as the solution of the following boundary value problem:

$$\begin{cases} \lambda^2\ \boldsymbol{\nabla}^2\widetilde{D} - \widetilde{D} + D = 0 & \\ \qquad\qquad \widetilde{D} = 0\ m & \text{on the coastlines} \\ \qquad\qquad \widetilde{D} = 200\ m & \text{on the shelfbreak} \end{cases} \tag{10}$$

where λ is a smoothing scale factor. This length scale corresponds to the length scale of the features we want to smooth. For the meshes displayed in this paper, we use a scale factor equal to $2.5\ km$. It must be stressed that this smoothed bathymetry is only used for the refinement mesh strategy and that the eco-hydrodynamical model can still be based on the original bathymetry field.

6 Concluding remarks

Mesh adaptivity can be used to generate efficient high-resolution unstructured meshes for the Great Barrier Reef taking advantage of the knowledge of the physics of the problem. From the bathymetry and the island distance, we build meshes on which finite element or control volume numerical simulations can be performed. It is possible to optimise the mesh with respect to several design parameters in order to be able to simulate small scale flow features along islands and reefs without the need to uniformly cover the whole domain with a fine resolution.

The analysis of the quality of the meshes by three quality gauges has been performed and demonstrates that high graded meshes can be obtained with good geometrical properties. The latter ensure good numerical conditioning of the hydrodynamical models solved with those grids. The selection of the

suitable design parameters will be tested in numerical simulations of the flow in the whole Great Barrier Reef.

Acknowledgements

Eric Deleersnijder and Emmanuel Hanert are a Research Associate and a Post-doctoral Researcher, respectively, with the Belgian National Fund for Scientific Research (FNRS). The present study was carried out within the scope of the project "A second-generation model of the ocean system", which is funded by the *Communauté Française de Belgique*, as *Actions de Recherche Concertées*, under contract ARC 04/09-316. This work is a contribution to the development of SLIM, the Second-generation Louvain-la-neuve Ice-ocean Model.

A Unstructured mesh generation

Generating unstructured mesh was the scope of a large number of works and softwares and is very well documented in the literature (e.g. Henry and Walters, 1993; Shewchuk, 1996 ; Frey and George, 2000). In this work, we use our own code to generate Delaunay-like triangulations (Legrand et al., 2000). It is based on the Watson-Bowyer incremental algorithm (Watson, 1981; Bowyer, 1981) and allows for a dynamical control of the element size, shape and orientation, which is achieved by introducing a prescribed target element metric.

The Watson-Bowyer algorithm generates triangulations by incrementally inserting each node of the final triangulation into an intermediate one. The insertion procedure is performed in two steps. The triangle containing the new site is first replaced by three new triangles and the quality of the new triangulation is then improved by swapping well-chosen edges.

The major steps of our mesh generation procedure are as follows:

- Starting from a large triangle containing the whole domain, boundary nodes are inserted.
- Once all boundary edges are created, useless triangles are removed.
- Then, additional nodes are created to obtain a mesh conformed to the target element size (Frey, 1987).
- Finally, the mesh quality is optimized by heuristic elliptic techniques that may be accompanied by edge swaps.

Algorithmic details as well as implementation issues are described in Legrand et al. (2000).

B The shore proximity function bounds

Demonstrating that the shore proximity function $\sigma(\mathbf{x})$ satisfies inequalities $0 \leq \sigma(\mathbf{x}) \leq 1$ is tantamount to see that the negative part of $\sigma(\mathbf{x}) - 0$ and the positive part of $\sigma(\mathbf{x}) - 1$ are zero. The former and the latter are defined as

$$[\sigma(\mathbf{x}) - 0]^- = \frac{(\sigma(\mathbf{x}) - 0) - |\sigma(\mathbf{x}) - 0|}{2} \tag{B.1}$$

and

$$[\sigma(\mathbf{x}) - 1]^+ = \frac{(\sigma(\mathbf{x}) - 1) + |\sigma(\mathbf{x}) - 1|}{2}, \tag{B.2}$$

respectively. To demonstrate that (B.1) and (B.2) actually are zero, inspiration may be found in Lewandowski (1997) or Deleersnijder et al. (2001). Accordingly, the Poisson equation (3) is multiplied by $[\sigma(\mathbf{x}) - 0]^-$ and, after integration by parts over the domain of interest Ω and substitution of the boundary conditions, the following integral is obtained:

$$\int_\Omega \left\{ \mu^2 \left| \boldsymbol{\nabla} \left[\sigma(\mathbf{x}) - 0\right]^- \right|^2 + \left| \left[\sigma(\mathbf{x}) - 0\right]^- \right| \left(1 + \left| \left[\sigma(\mathbf{x}) - 0\right]^- \right| \right) \right\} \, \mathrm{d}\Omega = 0. \tag{B.3}$$

All the terms of the integrand of (B.3) are positive and, yet, this integral is zero. This is possible if and only if $[\sigma(\mathbf{x}) - 0]^-$ is zero at every location $\mathbf{x}$ in the domain of interest.

To show that $[\sigma(\mathbf{x}) - 1]^+$ is also zero, a similar technique is resorted to. The counterpart of integral (B.3) is then

$$\int_\Omega \left\{ \mu^2 \left| \boldsymbol{\nabla} \left[\sigma(\mathbf{x}) - 1\right]^+ \right|^2 + \left(\left[\sigma(\mathbf{x}) - 1\right]^+ \right)^2 \right\} \, \mathrm{d}\Omega = 0, \tag{B.4}$$

implying that $[\sigma(\mathbf{x}) - 1]^+$ must be zero. QED.

References

Armsworth, P., Bode, L., 1999. The consequences of non-passive advection and directed motion for population dynamics. Proceedings of the royal Society of London Series A-Mathematical, Physical and Engineering Sciences 455, 4045–4060.

Assaker, R., 1998. Magnetohydrodynamics in crystal growth. Ph.D. thesis, Université catholique de Louvain.

Assaker, R., Van den Bogaert, N., Dupret, F., 1997. Time-dependent simulation of growth of large silicon crystal by the Czochralski technique using a turbulent model for melt convection. Journal of Crystal Growth 180, 450–460.

Bell, R., Elmetri, I., 1995. Ecological indicators of large-scale eutrophication in the Great Barrier Reef lagoon. Ambio 24, 208–215.

Bowyer, A., 1981. Computing Dirichlet tesselations. The Computer Journal 24 (2), 162–167.

Brasseur, P., Beckers, J.-M., Brankart, J.-M., Schoenauen, R., 1996. Seasonal temperature and salinity fields in the Mediterranean Sea: Climatological analyses of a historical data set. Deep-Sea Research I 43, 159–192.

Brinkman, R., Wolanski, E., Deleersnijder, E., McAllister, F., Skirving, W., 2002. Oceanic inflow from the Coral Sea into the Great Barrier Reef. Estuarine, Coastal and Shelf Science 54, 655–668.

Deleersnijder, E., Campin, J.-M., Delhez, E.J.M., 2001. The concept of age in marine modelling: I.Theory and preliminary model results. Journal of Marine Systems 28, 229–267.

Deleersnijder, E., Norro, A., Wolanski, E., 1992. A three-dimensional model of the water circulation around an island in shallow water. Continental Shelf Research 12, 891–906.

Dompierre, J., Vallet, M.-G., Labb, P., Guibault, F., 2003. On simplex shape measures with extension for anisotropic meshes. In: Workshop on mesh quality and dynamic meshing. Sandia National Laboratories - Livermore, CA, pp. 46–71.

Done, T., 1988. Simulations of the recovery of pre-disturbance size structure in populations of porites spp. damaged by crown-of-thorns starfish. Marine Biology 100, 51–61.

Foreman, M.G.G., Walters, R.A., Henry, R.F., Keller, C.P., Dolling, A.G., 1995. A tidal model for eastern Juan de Fuca Strait and the southern Strait of Georgia. Journal of Geophysical Research 100 (C1), 721–740.

Frey, P., George, P., 2000. Mesh generation : Application to finite elements. Hermes Science Publishing.

Frey, W., 1987. Selective refinement: A new strategy for automatic node placement in graded triangular meshes. International Journal for Numerical Methods in Engineering 24 (11), 2183–2200.

Hamner, W., Hauri, I., 1981. Effect of island mass: water flow and plankton pattern around a reef in the Great Barrier Reef lagoon. Limnology & Oceanography 26, 1084–1102.

Hanert, E., Le Roux, D.Y., Legat, V., Deleersnijder, E., 2005. An efficient Eulerian finite element for the shallow water equations. Ocean Modelling 10, 115–136.

Henry, R., Walters, R., 1993. Geometrically based, automatic generator for irregular networks. Communications in Numerical Methods in engineering

9, 555–566.

Jarosz, E., Blain, C.A., Murray, S.P., Inoue, M., 2005. Barotropic tides in the Bab el Mandab Straits — numerical simulations. Continental Shelf Research 25, 1225–1247.

Legrand, S., Legat, V., Deleersnijder, E., 2000. Delaunay mesh generation for an unstructured-grid ocean general circulation model. Ocean Modelling 2, 17–28.

Lewandowski, R., 1997. Analyse Mathématique et Océanographie. Masson(Paris).

Lewis, A., 2001. Great Barrier Reef depth and elevation model: GBRDEM. Technical Report 33, CRC Reef Research Centre Ltd, Townsville, Australia, 58 pp.

Pietrzak, J., Deleersnijder, E., Schroeter, J. (Eds.), 2005. The Second International Workshop on Unstructured Mesh Numerical Modelling of Coastal, Shelf and Ocean Flows. Ocean Modelling (special issue) 10, 1-252.

Shewchuk, J.R., 1996. Triangle: Engineering a 2d quality mesh generator and delaunay triangulator. In: First Workshop on Applied Computational Geometry (Philadelphia, Pennsylvania). Association for Computing Machinery, pp. 124–133.

Walters, R., 2005. Coastal ocean models: Two useful finite element methods. Continental Shelf Research 25, 775–793.

Watson, D., 1981. Computing the n-dimensional Delaunay tesselation with applications to Voronoi polytopes. The Computer Journal 24 (2), 167–172.

Wolanski, E., Asaeda, T., Tanaka, A., Deleersnijder, E., 1996. Three-dimensional island wakes in the field, laboratory and numerical models. Continental Shelf Research 16, 1437–1452.

Wolanski, E., Brinkman, R., Spagnol, S., McAllister, F., Steinberg, C., Skirving, W., Deleersnijder, W., 2003a. Advances in Coastal Modeling. Elsevier, Ch. Merging scales in models of water circulation: Perspectives from the Great Barrier Reef, pp. 411–429.

Wolanski, E., Doherty, P., Carleton, J., 1997. Directional swimming of fish larvae determines connectivity of fish populations on the Great Barrier Reef. Naturwissenschaften 84, 262–268.

Wolanski, E., Drew, E., Abel, K., O'Brien, J., 1988. Tidal jets, nutrient upwelling and their influence on the productivity of the algal Halimeda in the Ribbon Reefs, Great Barrier Reef. Estuarine, Coastal and Shelf Science 26, 169–201.

Wolanski, E., Hamner, W., 1988. Topographically controlled fronts in the ocean and their biological influence. Science 241, 177–181.

Wolanski, E., King, B., Spagnol, S., 1999. Perspectives in Integrated Coastal Zone Management. Springer-Verlag, Berlin, Ch. The implication of oceanographic chaos for coastal management, pp. 129–141.

Wolanski, E., Marshall, K., Spagnol, S., 2003b. Nepheloid layer dynamics in coastal waters of the Great Barrier Reef, Australia. Journal of Coastal Research 19, 748–752.

Wolanski, E., Richmond, R., McCook, L., 2004. A model of the effects of land-based, human activities on the health of coral reefs in the Great Barrier Reef and in Fouha Bay, Guam, Micronesia. Journal of Marine Systems 46, 133–144.

Wolanski, E., Spagnol, S., 2000. Pollution by mud of Great Barrier Reef coastal waters. Journal of Coastal Research 16, 1151–1156.

List of Figures

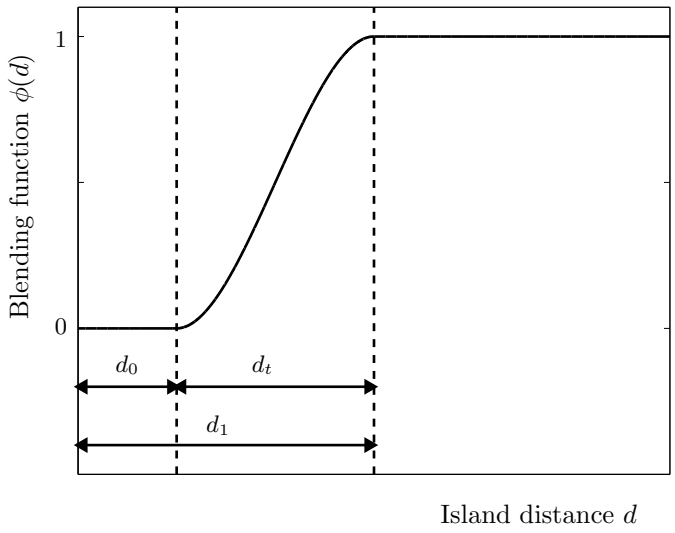

Fig. B.1. Definition of the geometrical parameters of the blending function $\phi(d)$.

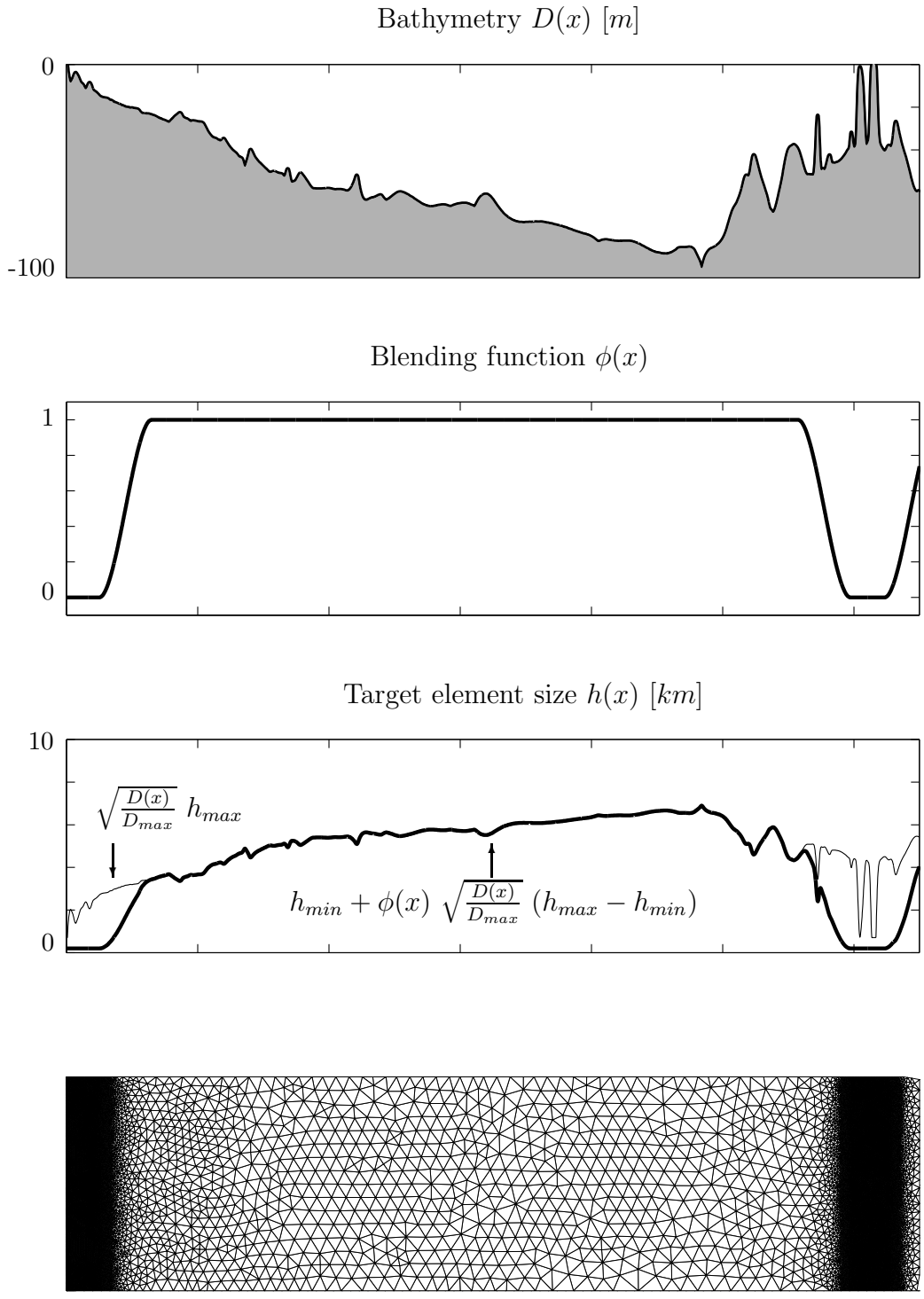

Fig. B.2. Target element size and generated mesh obtained by the blend of the bathymetry and the refinement required along the islands and reefs.

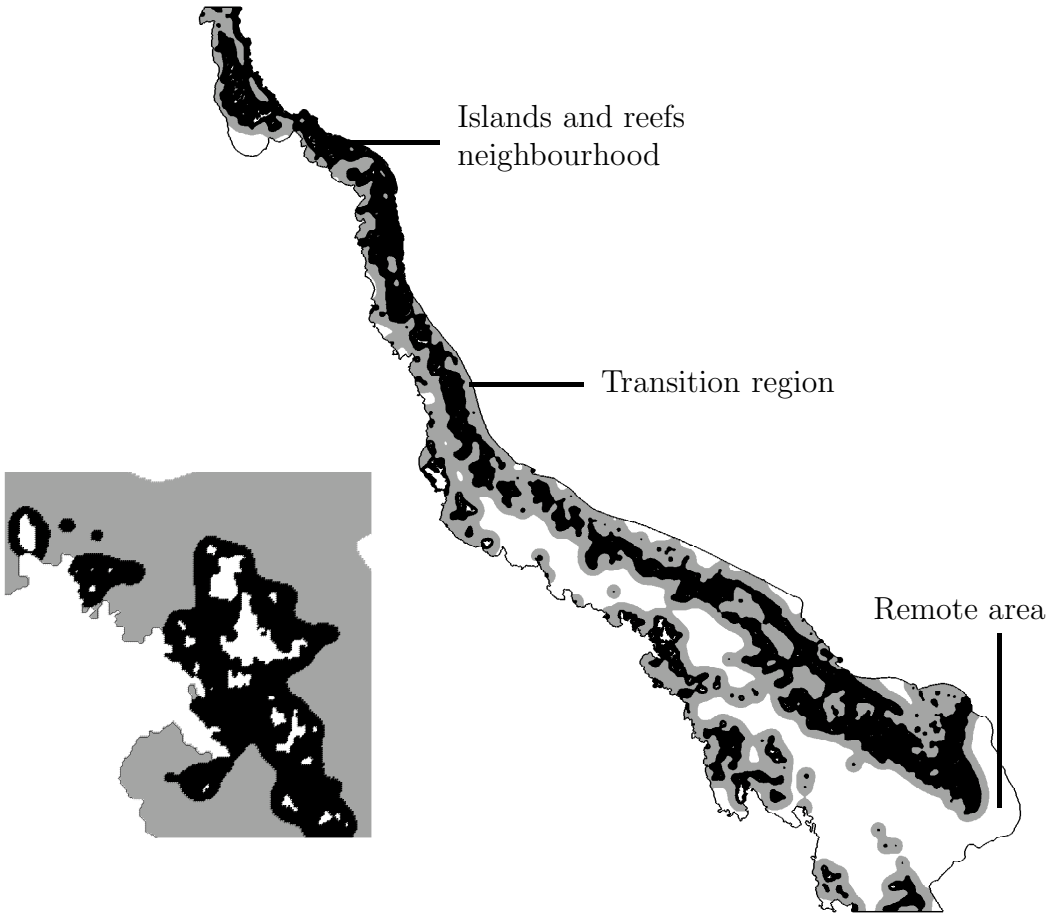

Fig. B.3. Partition of the domain into three regions. The dark area close to islands and reefs requires a fine discretization. The white part of the continental shelf far from islands and reefs is covered only by a coarse discretization. The grey area provides a smooth transition between the regions previously defined.

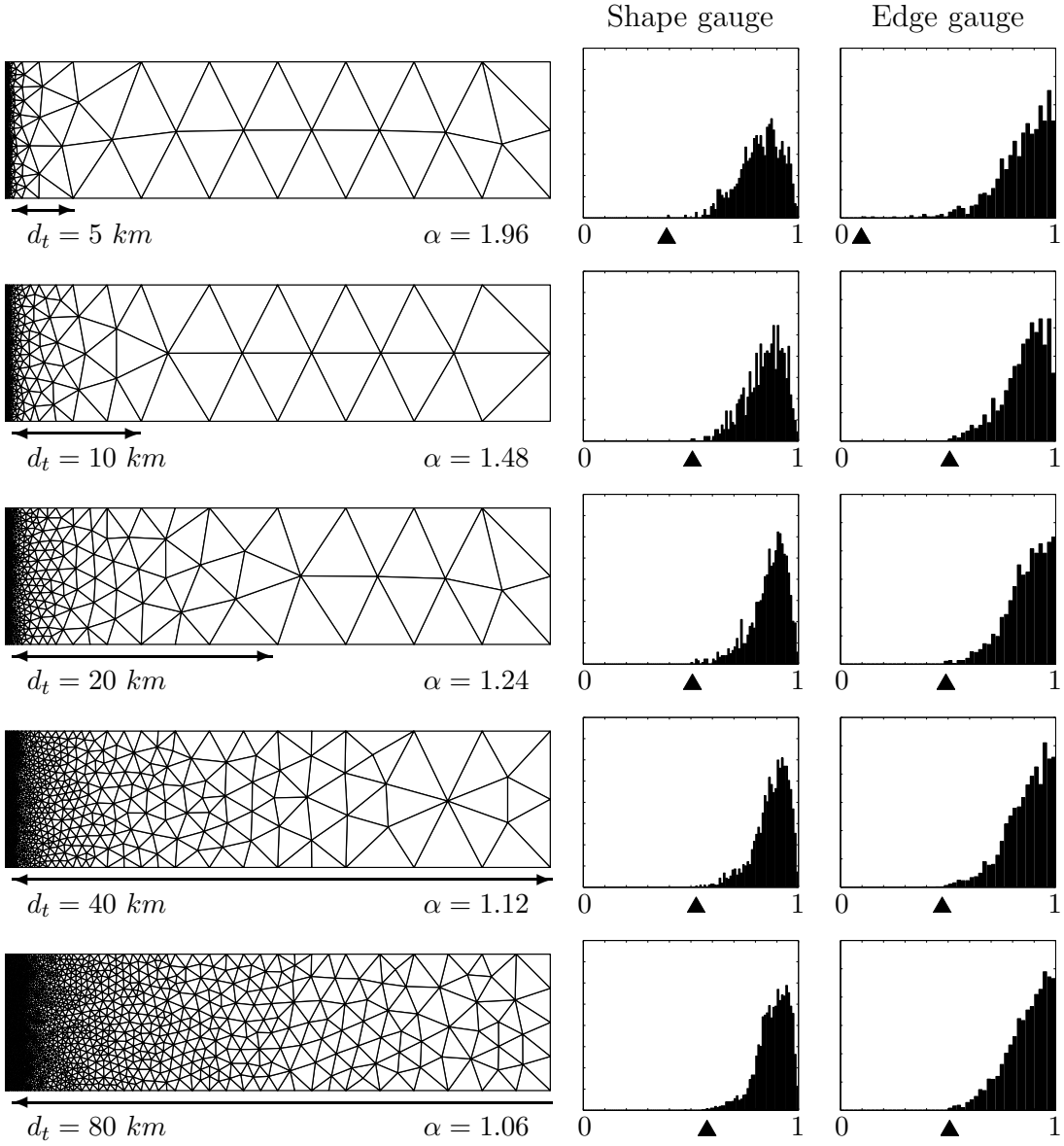

Fig. B.4. Impact of the transition distance on the generated meshes and on the normalized distributions of the shape gauge and the edge gauge. The black triangles point out the gauges value of the worst quality triangle. The smallest and biggest element sizes are 0.1 and 5 km, respectively.

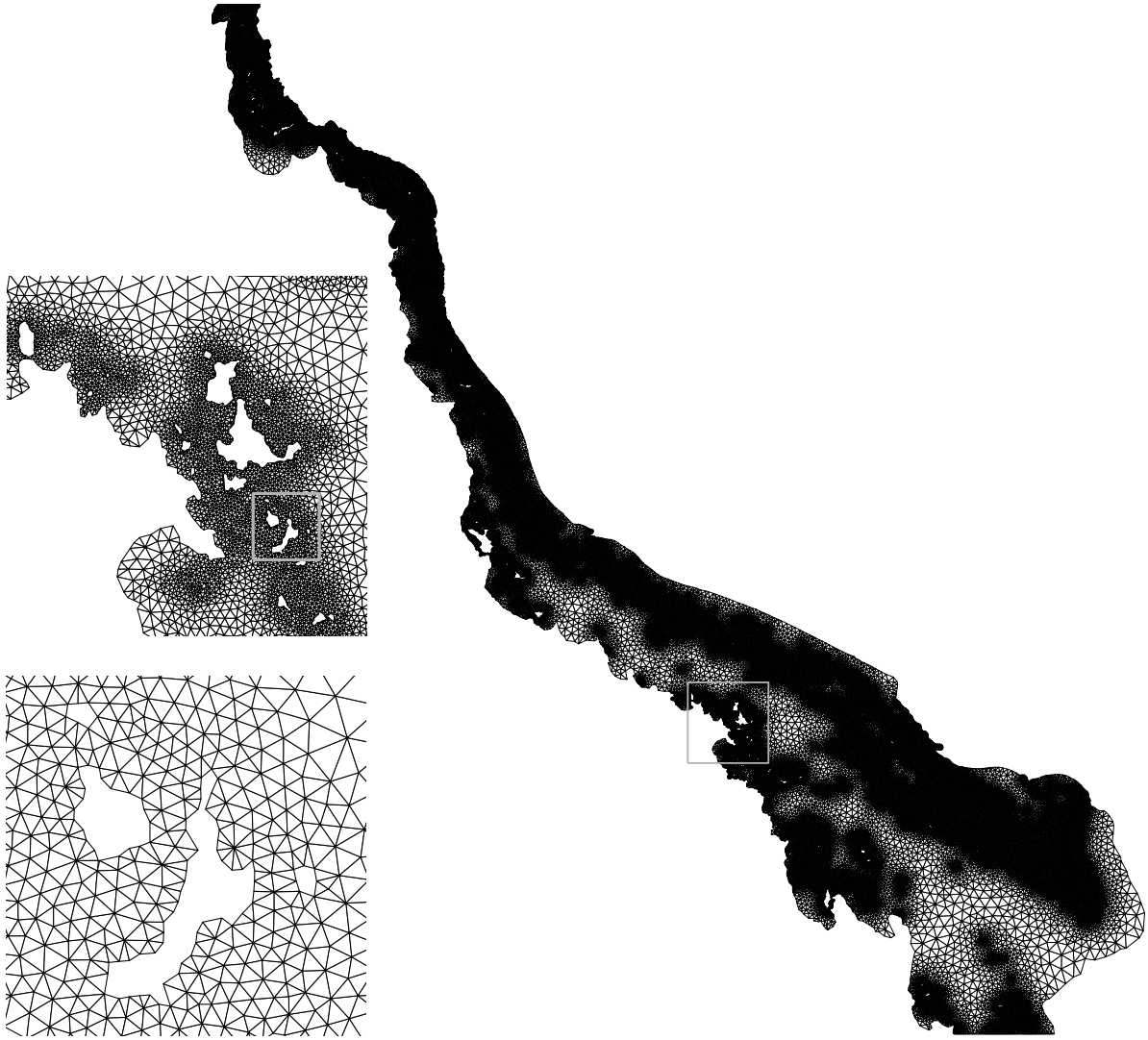

Fig. B.5. Mesh of the Great Barrier Reef with two recursive close up views illustrating the large spectrum of element sizes. The minimal and the maximal mesh sizes are 1 and 20 km, respectively. The number of elements and nodes are 95 843 and 184 142, respectively.

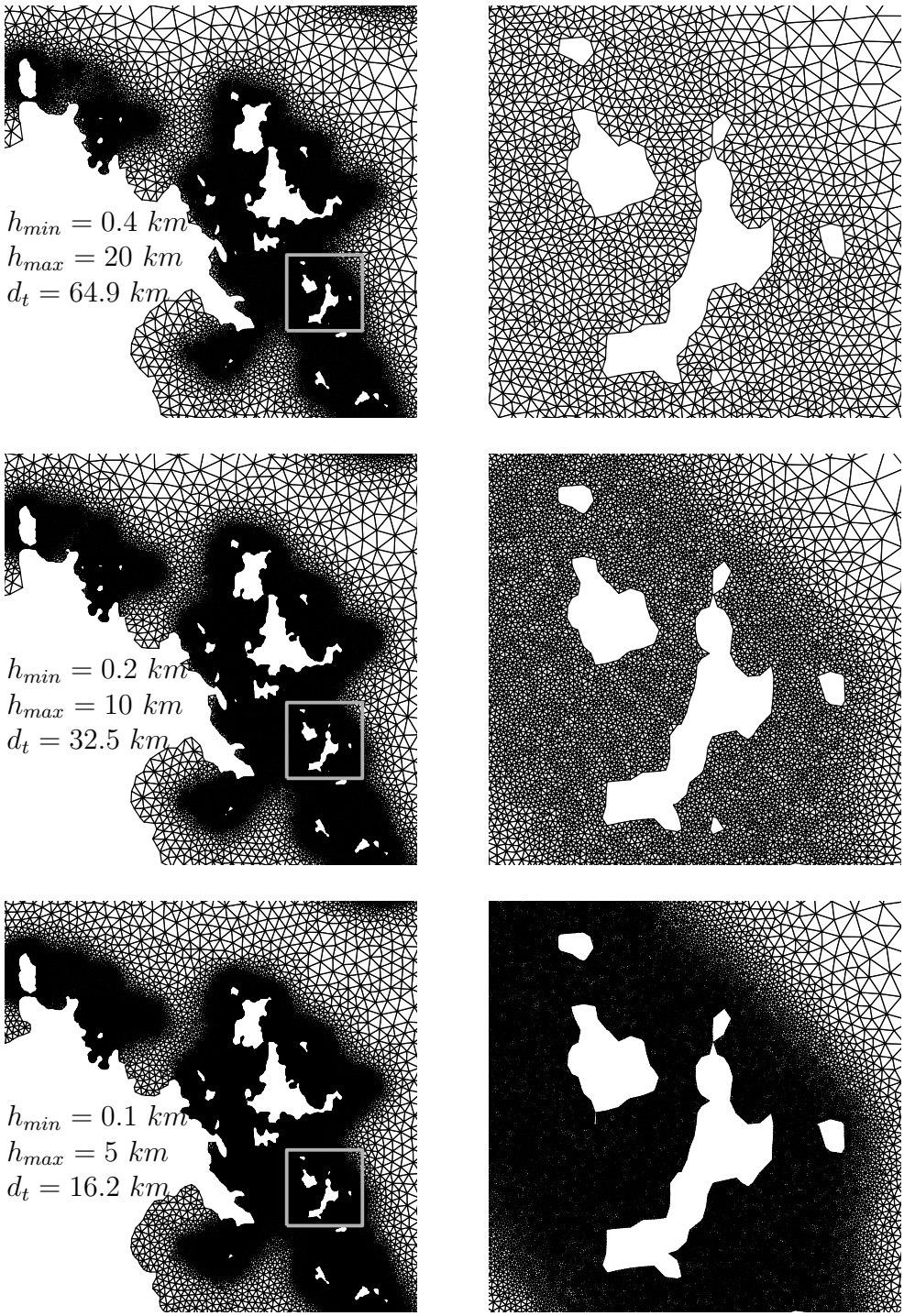

Fig. B.6. Meshes produced for a refinement analysis with sizes of h, $h/2$ and $h/4$ and the same geometrical parameters.